NJC

New Journal of Chemistry

A journal for new directions in chemistry

Accepted Manuscript

This article can be cited before page numbers have been issued, to do this please use: B. Goldfuss, E. Bruellingen and J. Neudoerfl, *New J. Chem.*, 2019, DOI: 10.1039/C9NJ02798J.

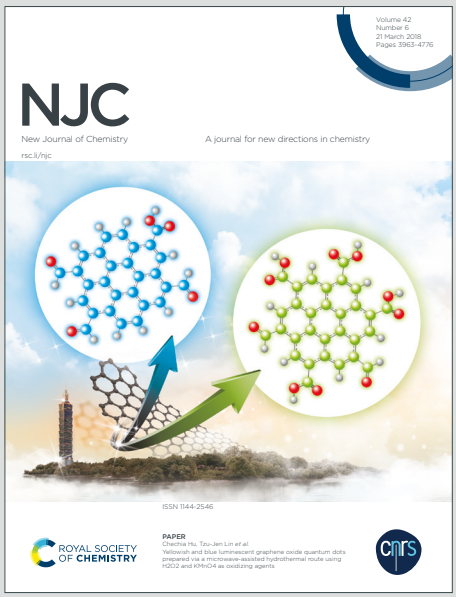

This is an Accepted Manuscript, which has been through the Royal Society of Chemistry peer review process and has been accepted for publication.

Accepted Manuscripts are published online shortly after acceptance, before technical editing, formatting and proof reading. Using this free service, authors can make their results available to the community, in citable form, before we publish the edited article. We will replace this Accepted Manuscript with the edited and formatted Advance Article as soon as it is available.

You can find more information about Accepted Manuscripts in the Information for Authors.

Please note that technical editing may introduce minor changes to the text and/or graphics, which may alter content. The journal's standard Terms & Conditions and the Ethical guidelines still apply. In no event shall the Royal Society of Chemistry be held responsible for any errors or omissions in this Accepted Manuscript or any consequences arising from the use of any information it contains.

View Article Online
DOI: 10.1039/C9NJ02798J

ARTICLE

Ligand's Electronegativity Controls Sense of Enantioselectivity in BIFOP-X Palladium-Catalyzed Allylic Alkylations

Received 00th January 20xx,
Accepted 00th January 20xx

DOI: 10.1039/x0xx00000x

www.rsc.org/

Eric Brüllingen, Jörg-Martin Neudörfl‡ and Bernd Goldfuss*

Palladium-catalyzed allylic alkylations of sodium dimethyl malonate with 1,3-diphenylallyl acetate, employing BIFOP-H (biphenylbisfencholphosphite) and analogue (i.e. BIFOP-X, X = D, Cl, CN, N_3) ligands, all yield (*S*)-enantiomeric products, while alkylations to cyclohexenyl acetate yield the (*R*)-enantiomeric C-C coupling product (up to 91% yield, 70% ee). The fluoro derivative BIFOP-F however, "switches" the sense of enantioselectivity yielding the (*R*)-enantiomer for 1,3-diphenylallyl acetate and the (*S*)-enantiomer for the cyclohexenyl acetate (up tp 92% yield, 67% ee). Computational analyzes of transition structures (M06-2X-D3/def2-TZVP//B3LYP-D3(BJ)/def2-SVP) for these Pd-catalyzed allylic alkylations, reproduce the experimental preference of BIFOP-H (and analogue BIFOP-X ligands) for (*R*)- or (*S*)-enantiomeric products of 1,3-diphenylallyl or cyclohexenyl acetate, respectively. The "F-switch" of the sense of enantioselectivity from BIFOP-H to BIFOP-F is also apparent computationally and is found (NBO-analyzes) to originate from lp(Pd) → σ*(P-O) or lp(Pd) → σ*(P-F) hyperconjugations. The higher electronegativity of F *vs.* H in BIFOP-X hence controls the sense of enantioselectivity of this Pd-catalyzed allylic alkylations.

Introduction

Palladium-catalyzed enantioselective allylic substitutions are an powerful tools for the formation of C-C bonds[1]. Enantioselective ligands (i.e. fenchol-based: arylfenchyl phosphites, FENOPs and biphenyl-2,2'-bisfenchol phosphites, BIFOPs or non-fencol-based ligands like Trost[1c] or Pfaltz-Helmchen-Williams[2]) are successfully employed for enantioselective metal-mediated-catalyzed reactions[3,4]. The difference of the ligands is presented in their different binding mode (P,P-ligands like Trost[4], P,N-ligands like Pfaltz-Helmchen-Williams[5] and monodentate P-ligands like the fenchol-based[3,4], Figure 1). Fenchols are the basis for entiopure, mixed anionic organo-lithium aggregates[5] as well as hydrogen-bonding Si-OH catalysts (i.e. $BIFOSi(OH)_2$)[5s]. FENOP and BIFOP ligands are used in Cu-catalyzed 1,4-additions[4,6a,7]. Despite its inherently reactive P-Hal function, BIFOP-Hal (Hal = F, Cl, Br) ligands prove to be suitable in palladium catalysts[6b,7]. In BIFOP-Hal (Hal= F, Cl, Br) Pd-catalysts, halide's electronegativity controls enantioselectivity in Pd-catalyzed cross-couplings[7]. Besides this BIFOP-H/F phenomenon, steering effects of fluorine-substituents on the stereochemical outcome have been observed[8,9].

In this work we present Pd-catalyzed C-C-coupling reactions, i.e. enantioselective allylic alkylations (Scheme 1), which show a surprising stereochemical-steering of the catalyst's fluorine substituent, stabilizing reversed Pd-allyl *exo-endo*-conformations[2a-f].

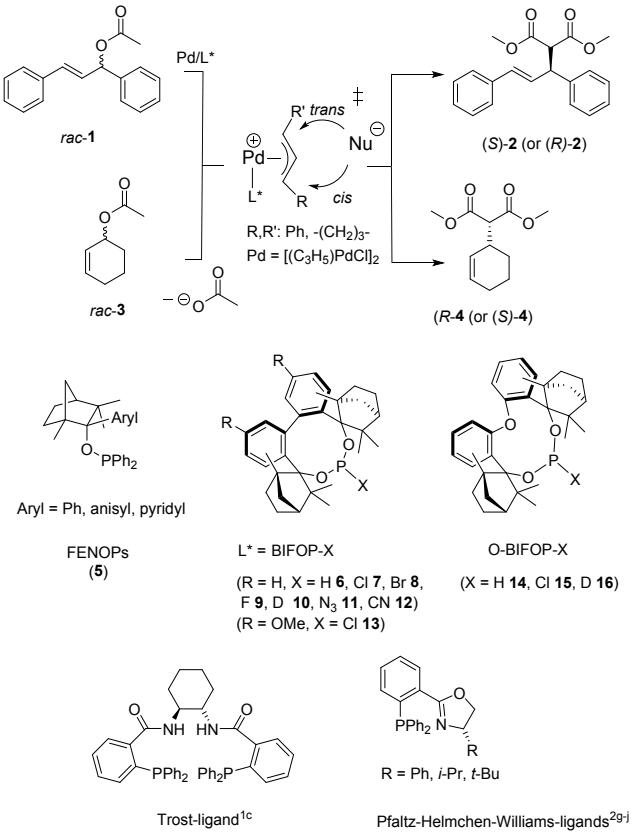

Department of Chemistry, University of Cologne, Organic Chemistry, Greinstr. 4, 50939 Cologne, Germany. Email: goldfuss@uni-koeln.de; Fax: +49 221 470 5057

† Electronic Supplementary Information (ESI) available: Detailed experimental data and copies of the HPLC and GC spectra. Detailed data of the X-ray crystal structure (CCDC 1862858-1886565) and detailed computational data (geometries, energies, imaginary frequencies, diagrams) are present. See DOI: 10.1039/x0xx00000x

‡ X-ray crystal structure analysis.

View Article Online
DOI: 10.1039/C9NJ02981

Scheme 1. Enantioselective Pd-catalyzed allylic alkylations and examples of fenchyl-based ligands (i.e. (O-)BIFOPs **6**-**16**) and established ligands like Trost's or Pfaltz-Helmchen-Williams.

Results and discussion

The Pd-BIFOP-H-catalyzed allylic alkylation of $Na(CH(CO_2CH_3)_2$ with (*rac*,*E*)-1,3-diphenyl allyl acetate (*rac*-**1**) yields (*S*,*E*)-dimethyl-2-(1,3-diphenylallyl)malonate (*S*)-**2** in up to 81% with 65% ee (Scheme 1, Table 1). The Pd-catalyzed allylic substitution is performed with three common methods to generate the nucleophile: The BSA method[10] (Table 1, entry 16), the *in situ* generation of the malonate ($CH(CO_2CH_3)_2$) with sodium carbonate (Na_2CO_3) analogue to ref.[11] (Table 1, entry 17) and the pre-formed sodium enolate ($Na(CH(CO_2CH_3)_2)^2$, Table 1, entry 13). All three methods yield the desired product with nearly equal results (cf. Table 1, entry 13, 16, 17). The highest yield and selectivity is obtained with pre-formed $Na(CH(CO_2CH_3)_2$ (Table 1, entry 13). At low temperatures (e.g. -30°C) the Pd-BIFOP-H-catalyzed allylic alkylation of $Na(CH(CO_2CH_3)_2)$ with 1,3-diphenyl acetate (*rac*-**1**) yields malonate (*S*)-**2** with loss of conversion but retaining stereocontrol (e.g. Table 1, 20°C, entry 13: 81% yield, 65% ee *vs.* -30°C, entry 14: 42% yield, 64% ee).

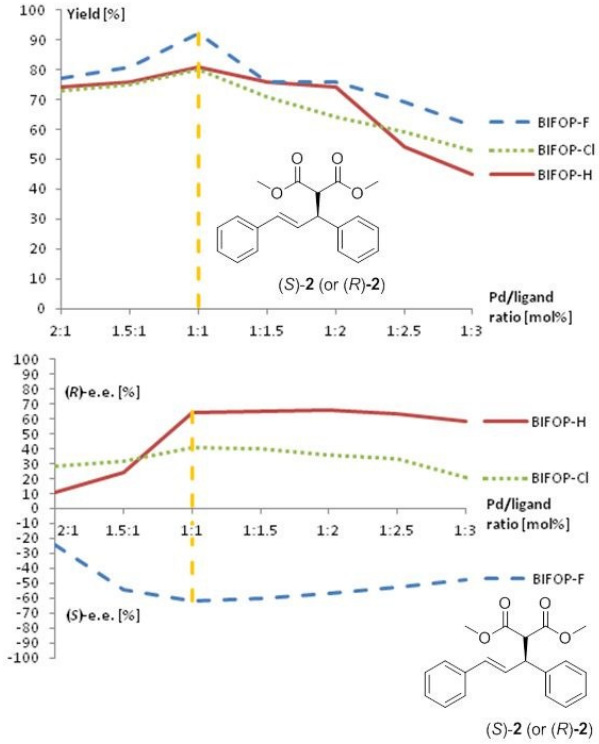

Figure 1. The active catalyst ratio of Pd-BIFOP-X (X = H **6**, Cl **7**, F **9**, cf. Scheme 2, Table 2).

At higher temperatures (e.g. 40°C) full conversions are achieved but with loss of stereocontrol (cf. Table 1, entry 15: 82% yield, 26% ee). Screening of the ether solvents (THF, dioxane, Et_2O, MTBE) reveals for THF forming moderate yield and entantioselectivity (52%, 55% ee, Table 1, entry 2). Dioxane improves yield but decreases the enantioselectivity (75%, 26% ee, Table 1, entry 3) while Et_2O provides nearly a complete loss of enantioselectivity (54%, 5% ee, Table 1, entry 4). MTBE is ordered between Et_2O and dioxane in yield and enantioselectivity (cf. Table 1, entry 5, 26%, 21% ee). Switching to polar solvents (MeCN, DMSO, DMF) shows that MeCN exceeds THF in yield while retaining enantioselectivity (cf. Table 1, entry 7, 87% yield, 56% ee), while DMSO decreases enantioselectivity (cf. Table 1, entry 10, 77% yield, 23% ee), nd DMF shows a complete loss of sterecontrol (cf. Table 1, entry 11, 46% yield, *rac*). Nucleophilic solvents like DMSO and DMF mights coordinate to Pd, affecting negatively the outcome of enantioselectivity. Apolar solvents (e.g. toluene, *n*-hexane) show a different behavior. While *n*-hexane generates decent yield and moderate enantioselecitivty (cf. Table 1, entry 9, 69% yield, 34% ee,), toluene is capable to form π-interactions with the Pd-center and thus hinders the catalysis to occur[12].

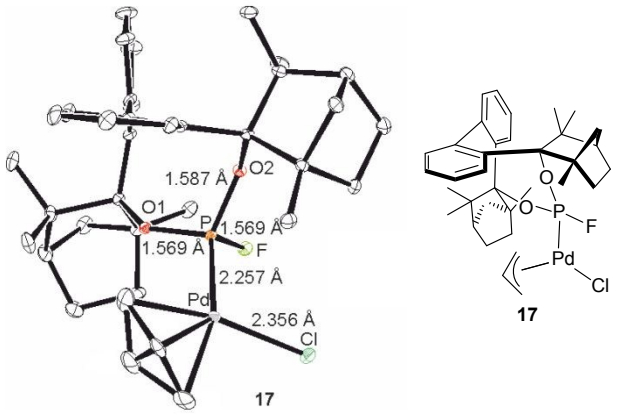

Figure 2. X-ray crystal structure (**17**, CCDC: 1886562) of $(C_3H_5)PdCl$ • BIFOP-F with dislocation of the (C_3H_5)-allyl unit. The hydrogens are omitted for clarity. The P-F distance of the blank BIFOP-F-ligand (**8**) in its X-ray crystal structure is 1.594 Å[7].

Finally, chlorinated solvents (e.g. DCM, 1,2-DCE) improve yield and enantioselectivity in comparison to THF (e.g. Table 1, entry 12, DCM, 72% yield, 62% ee). 1,2-DCE exceeds even DCM in the same catalysis (cf. Table 1, entry 13, 81% yield, 65% ee) delivering the best results of all solvents.

Different catalyst ratios ($[(C_3H_5)PdCl]_2$: BIFOP-X, X = H **6**, Cl **7**, F **9**, in mol%) have been examined (Figure 1, Table 2). In the Pd-BIFOP-X-catalyzed (X = H **6**, Cl **7**, F **9**) allylic alkylation of $Na(CH(CO_2CH_3)_2)$ to (*rac*,*E*)-1,3-diphenyl allyl acetate (*rac*-**1**) yielding (*S*, or *R*, *E*)-dimethyl 2-(1,3-diphenylallyl)malonate (*S*-, or *R*-**2**). The yield and enantioselectivity of (*S*, or *R*)-**2** increases with less amount of $[(C_3H_5)PdCl]_2$ used (Scheme 2, Figure 1, Table 2, e.g. entries 1-3) to a maximum at the ratio 1:1 (Scheme 2, Figure 1, Table 2, entries 3, 10, 17) and decreases with higher amounts of BIFOP-H (**6**) (Scheme 2, Figure 1, Table 2, e.g. entries 4-7). Thus, the background reaction is favoured with higher amounts of $[(C_3H_5)PdCl]_2$, catalyzing *rac*-**2**.

View Article Online
DOI: 10.1039/C9NJ02297J

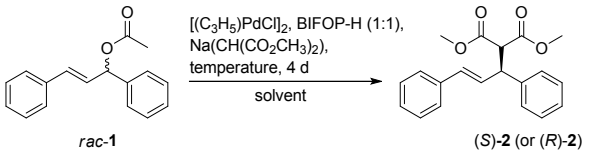

Scheme 2. Pd-catalyzed enantioselective allylic alkylation (Scheme 1). For evaluation see Table 1; for active catalyst ratio see Table 2; for ligand variation see Table 3.

Table 1. Evaluation of $Na(CH(CO_2CH_3)_2)$ to (*rac*,*E*)-1,3-diphenylallyl acetate (**1**) in enantioselective Pd-catalyzed allylic alkylation (Scheme 1, Scheme 2)[a].

Entry	Solvent	Temp. [°C]	Yield [%][b]	ee [%](*S*)[c]
1	THF	20	27	55
2	THF	20	52	55
3	dioxane	20	75	26
4	Et_2O	20	54	5
5	MTBE	20	26	21
6	MeCN	-30	34	31
7	MeCN	20	87	56
8	toluene	20	11	n.d.
9	*n*-hexane	20	69	34
10	DMSO	20	77	23
11	DMF	20	46	0
12	DCM	20	72	62
13	**1,2-DCE**	**20**	**81**	**65**
14	1,2-DCE	-30	42	64
15[d]	1,2-DCE	40	82	26
16[e]	1,2-DCE	20	78	63
17[f]	1,2-DCE	20	73	60

[a]1mol% $[(C_3H_5)PdCl]_2$, 1mol% BIFOP-H (**6**), 1.5 eq. of reagent $Na(CH(CO_2CH_3)_2)$, 4 d. [b]Isolated yield after silica gel column chromatography (ethyl acetate : *n*-hexane, 1:10). [c]Enantiomeric excess (ee) is determined *via* HPLC (Chiralpack® AD-H column, t_R = 19.7-24.8 min (*S*), t_R = 26.1-26.3 min (*R*)[13b]). [d]Reaction finished after 1 d. [e]The BSA method is used with $CH_2(CO_2CH_3)_2$ and KOAc instead of $Na(CH(CO_2CH_3)_2)$[10]. [f]*In situ* generation of $Na(CH(CO_2CH_3)_2)$ with Na_2CO_3 and $CH_2(CO_2CH_3)_2$ analogue to ref.[11].

Mixing $[(C_3H_5)PdCl]_2$ and BIFOP-F (**9**) in 1,2-DCE and *n*-heptane, colorless prisms of Pd-BIFOP-F (**17**, Figure 2) can be obtained. The X-ray crystal structure shows the dislocation of the allylic-unit (C_3H_5) due to the equilibrium of the *exo-endo*-conformers[9]. The catalytic performance of different BIFOP ligands (**6**-**16**, except **8**, Scheme 2, Table 3) is examined in the $[(C_3H_5)PdCl]_2$-catalyzed allylic alkylation of $Na(CH(CO_2CH_3)_2)$ to (*rac*,*E*)-1,3-diphenyl allyl acetate (*rac*-**1**) yielding (*S*, or *R*,*E*)-dimethyl 2-(1,3-diphenylallyl)malonate (*S*)-**2** (or (*R*)-**2**, Scheme 2, Table 3). BIFOP-H (**6**) yields (*S*)-**2** in up to 81% with 67% ee (Table 3, entry 1), while the ^{2}H-isotopic BIFOP-D (**10**) yields (*S*)-**2** in up to 84% with 66% ee (Table 3, entry 2). No isotopic effect is observed. BIFOP-Cl (**7**) yields (*S*)-**2** in up to 73% with 41% ee (Table 3, entry 3), while BIFOP-F (**9**) yields (*R*)-**2** in up to 92% with 66% ee (Table 3, entry 4). BIFOP-Cl (**7**) loses yield and enantioselectivity relative to BIFOP-X (X = H **6**, D **10**, F **9**). This means that BIFOP-X (X = H **6**, D **10**, F **9**) form more stable complexes with $[(C_3H_5)PdCl]_2$ than BIFOP-Cl (**7**).

BIFOP-N_3 (**11**) yields (*S*)-**2** in up to 83% with 12% ee (Table 3, entry 5) while BIFOP-CN (**12**) yields (*S*)-**2** in up to 78% with 11% ee (Table 3, entry 6). Pseudohalogenic substitutions at the BIFOP-moiety (e.g. N_3, CN) seem to have a detrimental effect to the enantioselectivities. This means, analogue to BIFOP-Cl (**7**), that BIFOP-N_3 (**11**) and BIFOP-CN (**12**) do not form stable complexes with $[(C_3H_5)PdCl]_2$.

Table 2. Selection of catalyst ratios of $[(C_3H_5)PdCl]_2$ • BIFOP-X (X = H **6**, Cl **7**, F **9**, Scheme 2, Figure 1)[a].

Entry	BIFOP-X	Ratio: $[(C_3H_5)PdCl]_2$ • BIFOP-X	Yield [%][b]	ee [%][c]
1	X = H (**6**)	2:1	74	11 (*S*)
2	X = H (**6**)	1.5:1	76	24 (*S*)
3	**X = H (6)**	**1:1**	**81**	**64 (*S*)**
4	X = H (**6**)	1:1.5	76	65 (*S*)
5	X = H (**6**)	1:2	74	66 (*S*)
6	X = H (**6**)	1:2.5	54	63 (*S*)
7	X = H (**6**)	1:3	45	58 (*S*)
8	X = F (**9**)	2:1	77	24 (*R*)
9	X = F (**9**)	1.5:1	81	54 (*R*)
10	**X = F (9)**	**1:1**	**92**	**62 (*R*)**
11	X = F (**9**)	1:1.5	76	60 (*R*)
12	X = F (**9**)	1:2	76	57 (*R*)
13	X = F (**9**)	1:2.5	69	53 (*R*)
14	X = F (**9**)	1:3	61	48 (*R*)
15	X = Cl (**7**)	2:1	73	28 (*S*)
16	X = Cl (**7**)	1.5:1	75	32 (*S*)
17	**X = Cl (7)**	**1:1**	**80**	**41 (*S*)**
18	X = Cl (**7**)	1:1.5	71	40 (*S*)
19	X = Cl (**7**)	1:2	64	36 (*S*)
20	X = Cl (**7**)	1:2.5	59	33 (*S*)
21	X = Cl (**7**)	1:3	53	21 (*S*)

[a]Ratio of x:y mol% $[(C_3H_5)PdCl]_2$, y mol% BIFOP-X (H **6**, Cl **7**, F **9**), 1.5 eq. of reagent $Na(CH(CO_2CH_3)_2)$, 4 d. [b]Isolated yield after silica gel column chromatography (ethyl acetate : *n*-hexane, 1:10). [c]Enantiomeric excess (ee) is determined via HPLC (Chiralpack® AD-H column, t_R = 19.7-24.8 min (*S*), t_R = 26.1-26.3 min (*R*)[10b]).

In contrast to BIFOP-X (X = H **6**, Cl **7**, D **10**, Scheme 1, Table 3, entry 1-3), O-BIFOP-X (X = H **14**, Cl **15**, D **16**, Scheme 1, Table 3, entry 7-9) generate more yield but less enantioselectivity. O-BIFOP-H (**12**) yields (*S*)-**2** in up to 89% with 58% ee (Table 3, entry 7) while O-BIFOP-D (**16**) yields (*S*)-**2** in up to 87% with 60% ee (Table 3, entry 8) and O-BIFOP-Cl (**15**) yields (*S*)-**2** in up to 81% with 40% ee (Table 3, entry 9).

The synthesis of O-BIFOP-F is attempted, starting with O-BIFOP-Cl (**15**), adding AgF, analogue to the synthesis of BIFOP-F (**9**)[7]. For this reaction the temperature of the reaction mixture is changed for each approach from 20°C to -78°C (20°C, 0°C, -20°C, -40°C, -78°C). After each attempt, the rearranged tricyclic product **18** is achieved instead of the desired product O-BIFOP-F (Scheme 4).

Table 3. Performance of BIFOP-X ligands in enantioselective $[(C_3H_5)PdCl]_2$-catalyzed allylic alkylation to (*rac*, *E*)-1,3-diphenyl allyl acetate (**1**,Scheme 2, Figure 1)[a].

Entry	Ligand	Yield [%][b]	ee [%][c]
1	BIFOP-H (**6**)	81	67 (*S*)
2	BIFOP- D (**10**)	84	66 (*S*)
3	X = Cl (**7**)	73	41 (*S*)
4 ("F-switch")	**X = F (9)**	**92**	**66 (*R*)**
5	X = N_3 (**11**)	83	12 (*S*)
6	X = CN (**12**)	78	11 (*S*)
7	O-BIFOP-H (**14**)	89	58 (*S*)
8	O-BIFOP-D (**16**)	87	60 (*S*)
9	O-BIFOP-Cl (**15**)	81	40 (*S*)
10	**$(MeO)_2$-BIFOP-Cl (13)**	**90**	**70 (*S*)**

[a]20°C, 1,2-DCE, 1 eq. $[(C_3H_5)PdCl]_2$ and 1 eq. BIFOP-X (X = H **6**, Cl **7**, F **9**, D **10**, N_3 **11**, CN **12**), $(MeO)_2$-BIFOP-Cl (**13**) or O-BIFOP-X (X = H **14**, Cl **15** D **16**) and 1.5 eq. of $Na(CH(CO_2CH_3)_2)$ to (*rac*, *E*)-1,3-diphenyl allyl acetate (**1**) yielding (*S*, or *R*, *E*)-dimethyl-2-(1,3-diphenylallyl)malonate (*S*)-**2** or (*R*)-**2**. [b]Isolated yield after silica gel column chromatography (ethyl acetate : *n*-hexane, 1:10). [c]Enantiomeric excess (ee) by HPLC (Chiralpack® AD-H column, t_R = 19.7-24.8 min (*S*), t_R = 26.1-26.3 min (*R*)[10b]).

The reason why O-BIFOP-X (X = H **14**, Cl **15**, D **16**) generate more yield but less enantioselectivity during catalysis, in contrast to BIFOP-X (X = H **6**, Cl **7**, D **10**), can be explained by the higher reactivity of O-BIFOPs in general, because of a larger bite-angle at the phosphor moiety[7], forming more stable complexes with $[(C_3H_5)PdCl]_2$. The loss of stereocontrol is caused by this angle. Relative to BIFOP-Cl (**7**) (cf. Table 3, entry 3, 73% yield, 41% ee), two MeO-groups increase the reactivity of the Pd-(MeO)2-BIFOP-Cl catalyst by lp(O)-conjugation (cf. Table 3, entry 10, 90% yield, 70% ee).

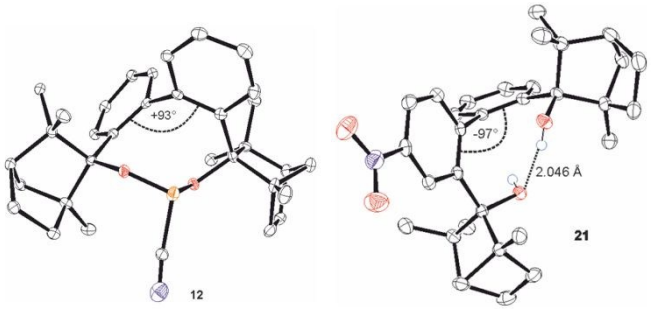

Figure 3. X-ray crystal structures of BIFOP-CN (**12**, CCDC: 1886565), and a backbone modified BIFOL *p*-NO_2-BIFOL (**21**, CCDC: 1886559). The hydrogens are omitted for clarity.

The mechanism for these rearrangements with formation of a carbo-cation at the fenchyl moiety and elimination of phosphonic acid (H_3PO_3), forming the tricyclic products, are discussed previously[16]. With $(MeO)_2$-BIFOP-Cl (**13**) an attempted variation of the BIFOP-X substituent (i.e. hydride, fluoride) was not successful.

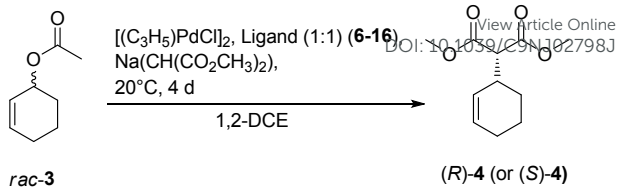

Scheme 3. Enantioselective $[(C_3H_5)PdCl]_2$-catalyzed allylic alkylation with (*rac*)-cyclohexenyl acetate (**3**, Scheme 1, Table 4).

Table 4. Performance of BIFOP-X ligands in enantioselective $[(C_3H_5)PdCl]_2$-catalyzed allylic alkylation to cyclohexenyl acetate **3** (Scheme 1, Scheme 3)[a].

Entry	BIFOP-X	Yield [%][b]	ee [%][c]
1	BIFOP-H (**6**)	83	64 (*R*)
2	BIFOP- D (**10**)	88	66 (*R*)
3	X = Cl (**7**)	71	54 (*R*)
4 ("F-switch")	**X = F (9)**	**82**	**67 (*S*)**
5	X = N_3 (**11**)	82	13 (*R*)
6	X = CN (**12**)	81	13 (*R*)
7	O-BIFOP-H (**14**)	84	64 (*R*)
8	O-BIFOP-D (**16**)	82	64 (*R*)
9	O-BIFOP-Cl (**15**)	80	56 (*R*)
10	**$(MeO)_2$-BIFOP-Cl (13)**	**91**	**67 (*R*)**

[a]20°C, 1,2-DCE, 1 eq. $[(C_3H_5)PdCl]_2$, 1 eq. BIFOP-X (X = H **6**, Cl **7**, F **9**, D **10**, N_3 **11**, CN **12**), $(MeO)_2$-BIFOP-Cl (**13**) or O-BIFOP-X (X = H **14**, Cl, **15** D **16**) and 1.5 eq. of $Na(CH(CO_2CH_3)_2)$ to (*rac*)-cyclohexenyl acetate (**3**) yielding (R, or S)-dimethyl-2-(cyclohexenyl) malonate (*R*)-**4** or (*S*)-**4**. [b]Isolated yield after silica gel column chromatography (ethyl acetate : *n*-hexane, 1:10). [c]Enantiomeric excess (ee) by chiral GC device with a CP-Chiralsil®-DEX-CB (25 m x 0.25 mm, 0.25 mm thickness, t_R = 22.4-22.8 min (*S*), t_R = 23.1-23.9 min (*R*)[14]) column.

The "F-switch" is found for the $[(C_3H_5)PdCl]_2$-catalyzed allylic alkylation of $Na(CH(CO_2CH_3)_2)$ with *rac*-cyclohexenyl acetate (*rac*-**3**) yielding (*S*)-dimethyl-2-(cyclohexenyl) malonate (*S*)-**4**, in case of BIFOP-F (**8**), or (*R*)-dimethyl-2-(cyclohexenyl) malonate (*R*)-**4** for the other BIFOP-X (X = H **6**, Cl **7**, F **9**, D **10**, N_3 **11**, CN **12**), $(MeO)_2$-BIFOP-Cl (**13**) or O-BIFOP-X (X = H **14**, Cl **15**, D **16**), too. BIFOP-H (**6**) yields (*R*)-**4** in up to 83% with 64% ee (Table 4, entry 1), while BIFOP-D (**10**) yields (*R*)-**4** in up to 88% with 66% ee (Table 4, entry 2). BIFOP-Cl (**7**) yields (*R*)-**4** in up to 71% with 54% ee (Table 4, entry 3), while BIFOP-F (**9**) yields (*S*)-**4** in up to 82% with 67% ee (Table 4, entry 4). BIFOP-N_3 (**11**) yields (*R*)-**4** in up to 82% with 13% ee (Table 4, entry 5) while BIFOP-CN (**12**) yields (*R*)-**4** in up to 81% with 13% ee (Table 4, entry 6). O-BIFOP-H (**14**) yields (*R*)-**4** in up to 84% with 64% ee (Table 4, entry 7) as well as O-BIFOP-D (**16**) which yields (*R*)-**4** in up to 82% with 64% ee (Table 4, entry 8). O-BIFOP-Cl (**15**) yields (*R*)-**4** in up to 80% with 56% ee (Table 4, entry 9). $(MeO)_2$-BIFOP-Cl (**13**) yields (*R*)-**4** in up to 91% with 69% ee (Table 3, entry 10) and appears to be the superior ligand in the $[(C_3H_5)PdCl]_2$-catalyzed allylic alkylation (cf. Table 3, Table 4).

Comparing the monodentate BIFOPs with the established P,N-ligands of Pfaltz-Helmchen-Williams, BIFOP-ligands are more bulky than the PHOX ligands but lack in transfer of stereoinformation forming lesser ee's.

View Article Online
DOI: 10.1039/C9NJ02798J

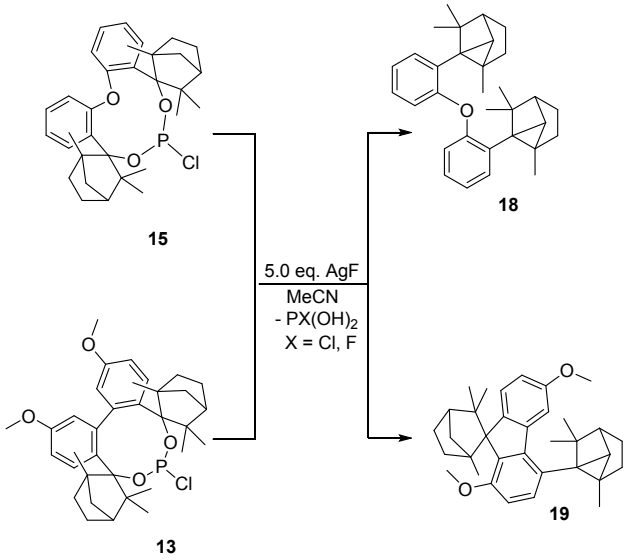

Scheme 4. Decomposition of O-BIFOP-Cl (**15**) to tricycle **18** and decomposition of $(MeO)_2$-BIFOP-Cl (**13**) to spiro[fenchyl-9-fluorene] **19** are analogue to the described decomposition in literature (cf. ref.[13]).

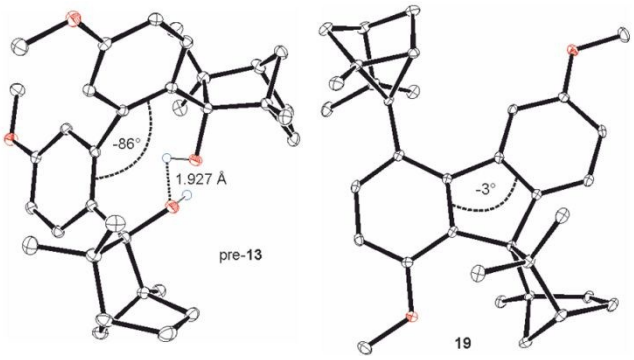

Figure 4. X-ray crystal structures of $(MeO)_2$-BIFOL (pre-**13**, CCDC: 1886561) and the decomposed product **19** (CCDC: 1886560). The hydrogen atoms attached to carbon atoms are omitted for clarity. The decomposition of **15** to **18** is described[13].

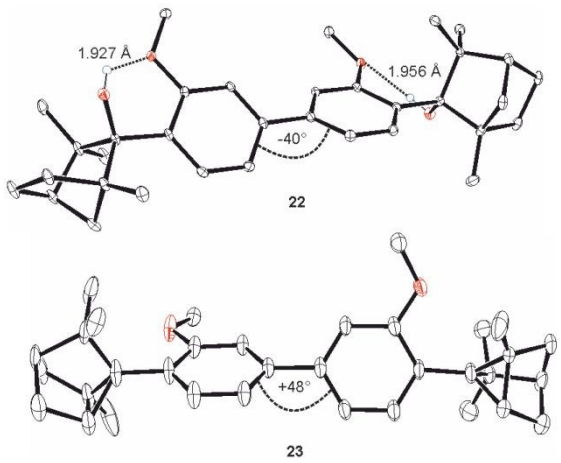

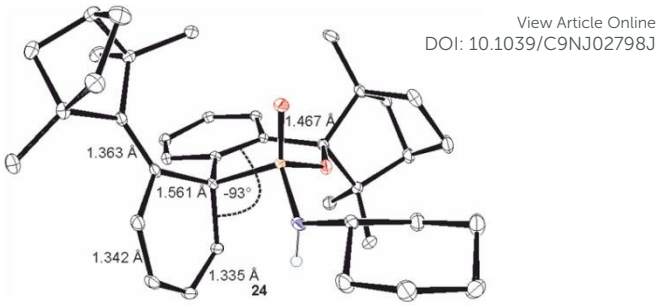

Figure 5. X-ray crystal structures of DIME-BIFOL (**22**, CCDC:1886564), it's decomposed product (**23**, CCDC: 1886558) and an intramolecular rearranged product of a biphenyl-2,2'-bisfenchol phosphoramidite (**24**, CCDC: 1886563). The hydrogen atoms attached to carbon atoms are omitted for clarity. The decomposition of diol **22** to tricyclic **23** is similar to the one described in literature[13].

Computational results

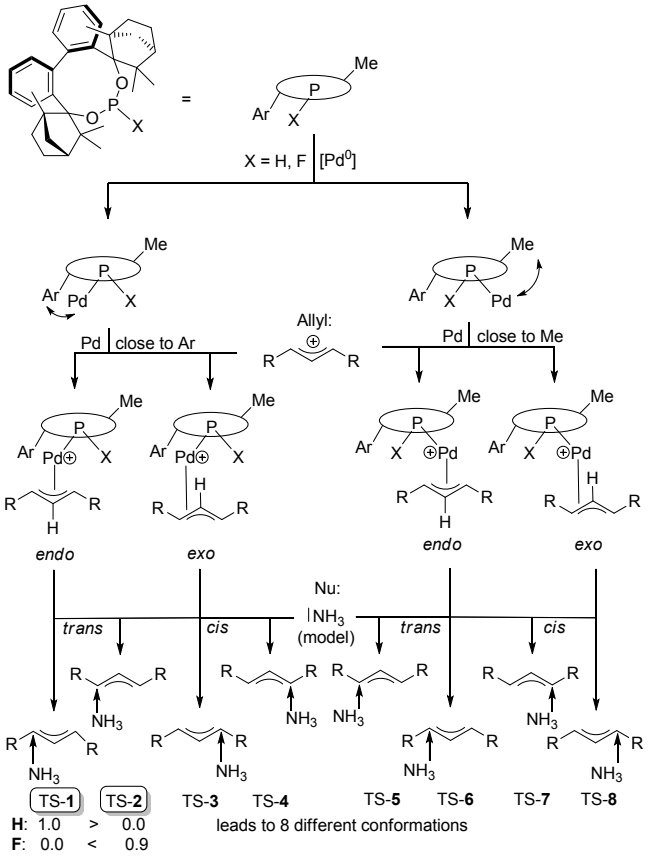

Scheme 5. Scheme of transition structures (R = Ph, $-(CH_2)_3-$) referring to the DFT-computations (H, F: TS-**1** to TS-**8**), to explain the origins of enantioselectivities (Table 5, Figure 6, Table 6, Figure 7).

$MeO)_2$-BIFOP-Cl (**13**) is easily synthesized by deprotonation of $(MeO)_2$-BIFOL (pre-**13**, Figure 4) and addition of PCl_3. $(MeO)_2$-BIFOL (pre-**13**, Figure 4) however cannot be obtained by lithiation with BuLi and TMEDA[4,5,6] of 3,3'-diemthoxy biphenyl, because DIME-BIFOL (**22**, Figure 5) is isolated instead. For a synthesis route of $(MeO)_2$-BIFOL (pre-**13**, Figure 4) please see

View Article Online
DOI: 10.1039/C9NJ02791

the SI. A reaction of **22** with PCl_3 leads to the carbo-cationic rearranged tricyclic product **23** (Figure 5), similar to the rearrangement of O-BIFOL (**15**) to the tricyclic product **18** (Scheme 3, Figure 4) or the rearrangement of $(MeO)_2$BIFOP-Cl (**13**) to spiro[fenchyl-9-fluorenyl] product **19** (Figure 4)[13].

The origins of enantioselectivity are considered by eight different conformations (Scheme 5). These catalyst-conformations differ with the Pd-core close to a Ph-group of the biaryl backbone or close to a Me-group of the fenchyl moiety (Scheme 2). The allyl cation can be orientated in an *exo*-conformation (*exo* means, the H of the C2 of the allylic(C_3H_5)-group is pointing *upwards*), or an *endo*-conformation (*endo* means, the H of the C2 of the allylic(C_3H_5)-group is pointing *downwards*, Scheme 5). The nucleophilic attack can occur on the C1 (*trans*-attack compared to phosphor, Scheme 1) or C3 (*cis*-attack compared to phosphor, which is mostly unfavoured, cf. Scheme 1) of the allyl(C_3H_5)-unit[9], leading to eight different possibilities for either BIFOP-H (**6**) or BIFOP-F (**9**) (Scheme 5).

Table 5. Computed transition structures (TS) of attached (*E*)-1,3-diphenyl allyl acetate (**1**) for BIFOP-X (X = H **6**; F **9**, Scheme 1, Scheme 5, Figure 6)[a].

TS (*pro*(*R*/*S*))[b]	Conformer (Ar- or Me-orientated)	Imag. Freq. [cm-1]	ΔG_{rel} [kcal/mol]	Boltzmann distribution [%]
H: TS-2 (*S*)	**(Ar)-*trans-exo***	**-301.94**	**0.0**	**56.00**
TS-**1** (*R*)	(Ar)- *trans-endo*	-282.73	1.0	19.07
TS-**3** (*S*)	(Ar)-*cis-endo*	-311.86	1.3	13.80
TS-**4** (*R*)	(Ar)- *trans-exo*	-294.38	1.5	11.12
TS-**6** (*R*)	(Me)-*trans-endo*	-301.94	11.0	<0.01
TS-**7** (*S*)	(Me)-*cis-endo*	-311.86	11.1	<0.01
TS-**5** (*R*)	(Me)-*trans-exo*	-282.73	11.5	<0.01
TS-**8** (*S*)	(Me)-*cis-exo*	-294.38	12.5	<0.01
F: TS-1 (*R*)	**(Ar)-*trans-endo***	**-291.93**	**0.0**	**53.33**
TS-**2** (*S*)	(Ar)-*trans-exo*	-302.23	0.9	20.22
TS-**4** (*R*)	(Ar)-*cis-exo*	-289.62	1.2	14.64
TS-**3** (*S*)	(Ar)-*cis-endo*	-311.86	1.4	11.80
TS-**6** (*R*)	(Me)-*trans-exo*	-302.23	10.2	<0.01
TS-**7** (*R*)	(Me)-*cis-endo*	-320.94	10.6	<0.01
TS-**5** (*S*)	(Me)-*trans-endo*	-291.93	10.7	<0.01
TS-**8** (*S*)	(Me)-*cis-exo*	-289.62	11.2	<0.01

[a]M06-2X-D3/def2-TZVP//B3LYP-D3(BJ)/def2-SVP, 293.15 K, p = 1 bar, gas phase. [b]The change of stereochemistry resulting from the NH_3-nucleophile is switched to match the C-nucleophile dimethylmalonate for the 1,3-diphenylallyl acetate (**1**, Figure 6).

The bent structure of the ligand attached to the Pd-core results from a strong π-backdonation[15]. The transition structures (**H**: TS-**1**, TS-**2** and **F**: TS-**1**, TS-**2**, Scheme 5, Table 5, Figure 6 and Table 6) are the crucial (energetically favoured) transition structures of BIFOP-H (**6**) and BIFOP-F (**9**), which are responsible for the enantioselectivity (cf. experimental data Table 3, Table 4). Comparing the conformers (Table 5), **H**: TS-**2**; **F**: TS-**1** and **H**: TS-**1b**; **F**: TS-**2b** (Table 6), there has to be a reason of the change in stereochemistry (cf. **H**: TS-**1** > TS-**2**; **F**: TS-**1** < TS-**2**, Scheme 5, Table 5, Figure 6 and **H**: TS-**1b** < TS-**2b**; **F**: TS-**1b** > TS-**2b**, Scheme 5, Table 6, Figure 7). The same results of favourizing the crucial transition structures are found by switching the nucleophile of NH_3 to the C-nucleophile diphenylmalonate (**H**: TS-**1c** < TS-**2c**; **F**: TS-**1c** > TS-**2c** and **H**: TS-**1d** < TS-**2d**; **F**: TS-**1d** < TS-**2d**, Table 7). An explanation is the higher electronegativity of F *vs*. H in the P-X (X = H, F) moiety, such governance of electronegativity has been studied[3,7]. Strong negative hyperconjugation is known for fluorine substituents, stabilizing normally less favoured conformations and thus altering the stereochemistry in organo- and metal-mediated catalyzes[8].

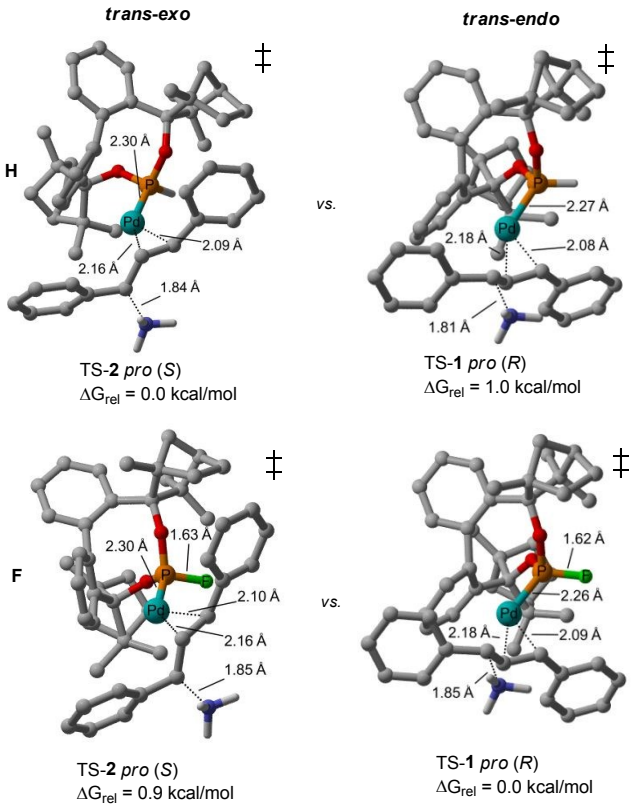

Figure 6. Computed crucial transition structures of (*E*)-1,3-diphenylallyl acetate (**1**) • Pd • BIFOP-X (X = H **6**, or F **9**, cf. Table 5).

Table 6. Computed transition structures (TS) of attached cyclohexenyl acetate (**3**) for BIFOP-X (X = H **6**; F **9**, Scheme 1, Scheme 5, Figure 7)[a].

TS (*pro*(*R*/*S*))	Conformer (Ph- or Me-orientated)	Imag. Freq. [cm-1]	ΔG_{rel} [kcal/mol]	Boltzmann distribution [%]
H: TS-1b (*R*)	**(Ar)-*trans-endo***	**-307.38**	**0.0**	**55.37**
TS-**4b** (*R*)	(Ar)-*cis-exo*	-322.47	0.5	32.31
TS-**2b** (*S*)	(Ar)-*trans-exo*	-308.51	1.6	9.88
TS-**3b** (*S*)	(Ar)-*cis-endo*	-322.44	2.9	2.43
F: TS-2b (*S*)	**(Ar)-*trans-exo***	**-307.33**	**0.0**	**59.46**
TS-**1b** (*R*)	(Ar)-*trans-endo*	-308.72	0.8	25.11
TS-**3b** (*S*)	(Ar)-*cis-endo*	-324.23	1.5	11.82
TS-**4b** (*R*)	(Ar)-*cis-exo*	-321.17	2.6	3.62

[a]M06-2X-D3/def2-TZVP//B3LYP-D3(BJ)/def2-SVP, 293.15 K, p = 1 bar, gas

View Article Online
DOI: 10.1039/C9NJ02798J

phase in kcal/mol.

A computational scan (B3LYP-D3(BJ)/def2-SVP) of a simpler model system **20**-X (X = H, F, Cl) reveals electronically preferred conformations (Figure 8, Table 8). For **20**-(H, Cl), two *exo*-minima as well as two *endo*-maxima (Figure 8) are computed.

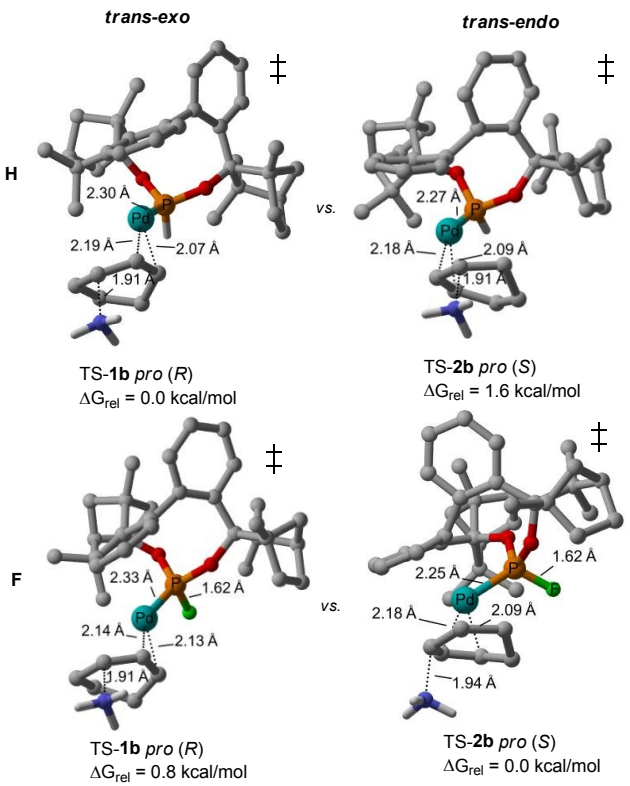

Figure 7. Computed crucial transition structures of cyclohexenyl acetate (**3**) • Pd • BIFOP-X (X = H **6**, or F **9**, cf. Table 5).

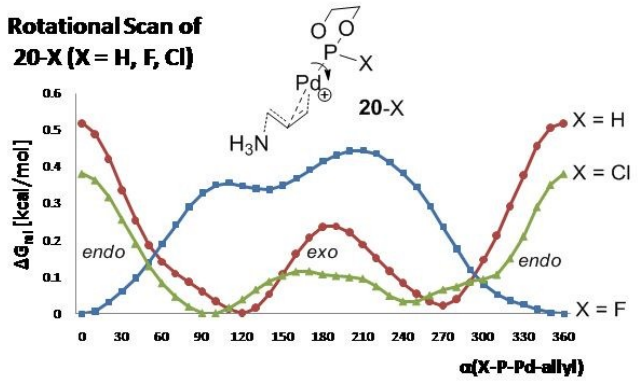

Figure 8. Computation (B3LYP-D3(BJ)/def2-SVP) of rotational (dihedral, (H,F,Cl)-P-Pd-allyl) scan of complex **20**-(H, F, Cl), representing the energy profiles (cf. Table 5).

Table 7. Computed transition structures (TS) of attached cyclohexenyl acetate (**3**, TS-**1c**,**2c**) or diphenylallyl acetate (**1**, TS-**1d**,**2d**) for BIFOP-X (X = H **6**; F **9**, Scheme 1, Scheme 5, Figure 9)[a].

TS (*pro*(*R*/*S*))	Conformer (Ph- or Me-orientated)	Imag. Freq. [cm-1]	ΔG_{rel} [kcal/mol]
H: TS-1c (*R*)	**(Ar)-*trans-endo***	**-173.12**	**0.0**
TS-**2c** (*S*)	(Ar)-*trans-exo*	-218.71	0.5
F: TS-2c (*S*)	**(Ar)-*trans-exo***	**-291.04**	**0.0**
TS-**1c** (*R*)	(Ar)-*trans-endo*	-195.76	0.7
H: TS-2d (*S*)	**(Ar)-*trans-exo***	**-239.20**	**0.0**
TS-**1d** (*R*)	(Ar)-*trans-endo*	-235.93	0.7
F: TS-1d (*R*)	**(Ar)-*trans-endo***	**-241.76**	**0.0**
TS-**2d** (*S*)	(Ar)-*trans-exo*	-230.67	0.7

[a]M06-2X-D3/def2-TZVP//B3LYP-D3(BJ)/def2-SVP, 293.15 K, p = 1 bar, gas phase in kcal/mol.

Negative hyperconjugation from the Pd-lp donor is favoured with the stronger σ*(P-O) acceptor rather than the σ*(P-X, X = H, Cl) unit (Table 8). The fluoro substituent in **20**-F gives rise to only one (global) *endo*-minimum and one *exo*-maximum, because of the stronger acceptor behavior of σ*(P-F) over σ*(P-O, Figure 8). The electronical difference between the oxygen in σ*(P-O) and fluorine in σ*(P-F) gives rise to the stereochemical switch in the experiments, because fluorine exceeds the influence of the σ*(P-O) changing the stereochemistry by stabilizing the generally less favoured complex, instead. Thus the sense of enantioselectivity is changed. This hypothesis is further approved by a rotatory scan of the (allyl)Pd-P-X (X = H, Cl, F) dihedral showing for **20**-(H, Cl) nearly the same graphical behavior, while **20**-F is showing a different one (Figure 8). The only difference between **20**-Cl and **20**-F is the higher electronegativity of fluorine over chlorine. This evidence explains the experimental results (cf. experimental: Table 3, Table 4, entry 4 with theoretical: Figure 8). NBO-analyzes reveal that this F-switch arises from hyperconjugation lp(Pd)→σ*(P-O) influenced by the high electronegativity of fluorine (Figure 8, Table 8).

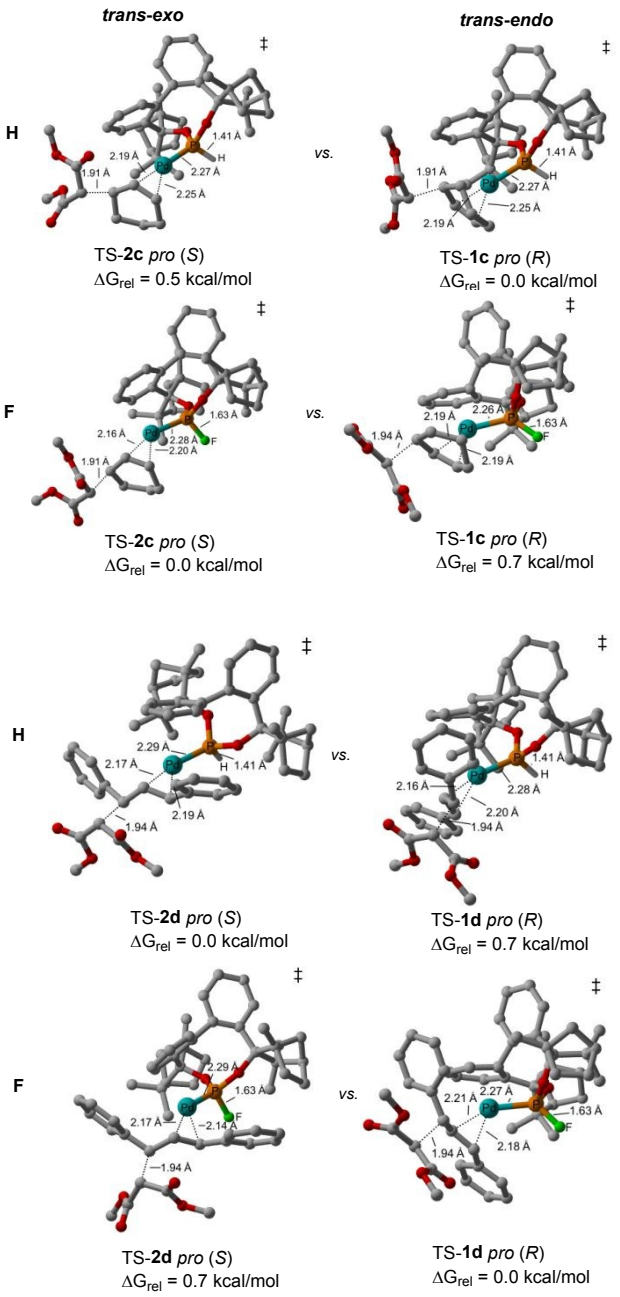

Figure 9. Computed crucial transition structures of acetate (1 and 3) • Pd• BIFOP-X (X = H 6, or F 9, with diphenylmalonate as nucleophile cf. Table 7).

Table 8. NBO-analyzes: stabilizing hyperconjugation of the model- (**20**-H, F, Cl) and "real"-(TS-**1**,**2**; TS-**1b**,**2b**;TS-**1c**,**2c**; TS-**1d**,**2d**) complex (Figure 8, Table 5, Table 6, Table 7)[a].

View Article Online
DOI: 10.1039/C9NJ02788J

Conformer (model *vs* "real")	NBO lp(Pd) → σ*(P-O) [kcal/mol][b]	Dihedral angle (allyl)Pd-P-(H, Cl, F) [°]	ΔG_{rel} [kcal/mol]
20-H (*exo-trans*)	**8.4**[c]	187.5	**0.0**
20-H (*endo-trans*)	8.5	15.5	0.1
20-Cl (*exo-trans*)	**8.3**[c]	168.6	**0.0**
20-Cl (*endo-trans*)	8.3	24.3	0.3
20-F (*endo-trans*)	**7.5**	22.9 ("**F-switch**")	**0.0**
20-F (*exo-trans*)	7.2	202.3	0.7
H: TS-**2** (*exo-trans*)	**7.6**	110.3	**0.0**
TS-**1** (*endo-trans*)	3.2	1.6	1.0
F: TS-**1** (*endo-trans*)	**8.0**	1.9 ("**F-switch**")	**0.0**
TS-**2** (*exo-trans*)	6.6	110.5	0.9
H: TS-**1b** (*endo-trans*)	**7.9**	107.7	**0.0**
TS-**2b** (*exo-trans*)	7.1	20.0	1.6
F: TS-**2b** (*exo-trans*)	**7.3**	14.3 ("**F-switch**")	**0.0**
TS-**1b** (*endo-trans*)	4.5	122.6	0.8
H: TS-**1c** (*endo-trans*)	**10.1**	179.8	**0.0**
TS-**2c** (*exo-trans*)	8.8	168.1	0.5
F: TS-**2c** (*exo-trans*)	**9.2**	24.3 ("**F-switch**")	**0.0**
TS-**1c** (*endo-trans*)	4.9	19.1	0.7
H: TS-**2d** (*exo-trans*)	**13.3**	95.6	**0.0**
TS-**1d** (*endo-trans*)	10.7	40.3	0.7
F: TS-**1d** (*endo-trans*)	**9.2**	19.7 ("**F-switch**")	**0.0**
TS-**2d** (*exo-trans*)	8.0	20.4	0.7

[a]M06-2X-D3/def2-TZVP//B3LYP-D3(BJ)/def2-SVP, T = 293.15 K, p = 1 bar, gas phase in kcal/mol. [b]Hyperconjugation: lp(Pd)->σ*(P-O) is mainly responsible for the stabilizing effect. For a comparison of the different hyperconjugations please see the SI. [c]The hyperconjugation lp(Pd)→σ*(allyl) exceeds the lp(Pd)→σ*(P-O) in this specific case. For a comparison of the different hyperconjugations please see the SI.

View Article Online
DOI: 10.1039/C9NJ02790D

Conclusions

Palladium-catalyzed allylic alkylations of sodium dimethyl malonate with (*rac*,*E*)-1,3-diphenylallyl acetate (**1**), employing BIFOP-X ligands (i.e. X = H **5**, Cl **7**, D **10**, N_3 **11**, CN **12**) yield (*S*,*E*)-dimethyl-2-(1,3-diphenylallyl) malonate (*S*)-**2** (up to 92%, 70% ee, cf. Scheme 2, Table 3), while alkylations with cyclohexenyl acetate yield (*R*)-dimethyl-2-(cyclohexenyl) malonate (*R*)-**4** (up to 91%, 67% ee, cf. Scheme 3, Table 4). Employed ligands for these Palladium-catalyzed allylic alkylations are BIFOP-X (X = H **5**, Cl **7**, F **9**), O-BIFOP-X (X = H **14**, Cl **15**) and newly synthesized ligands BIFOP-X (X = D **10**, N_3 **11**, CN **12**), $(MeO)_2$-BIFOP-Cl (**13**) and O-BIFOP-D (**16**). During the syntheses of new $(MeO)_2$-BIFOP-X (X = H) ligands, carbo-cationic rearrangements are found at the fenchyl moieties (spiro[fenchyl-9-fluorene] **19** and tricyclic product **23**, cf. ref. 13). Evaluation of catalyst ratios is achieved by variation of $[(C_3H_5)PdCl]_2$ and BIFOP-X (X = H **6**, Cl **7**, F **9**) in different amounts (3:1 to 1:3) and employing these amounts in the Pd-catalyzed allylic alkylation of $Na(CH(CO_2Me)_2)$ with 1,3-diphenylallyl acetate (**1**) yielding malonate (*S*)-**2** (or (*R*)-**2**, cf. Figure 1, Scheme 2, Table 2). This evaluation reveals a 1:1 ratio as optimized condition (Figure 1). This 1:1 ratio can also be seen at the isolated X-ray crystal structure of $(C_3H_5)PdCl$ • BIFOP-F (**17**, Figure 2). $(MeO)_2$-BIFOP-Cl (**13**) affords the best results of all tested ligands (90% yield, 70% ee, cf.Tables 3, 4 entries 10). O-BIFOP-D (**16**) affords similar results as O-BIFOP-H (**14**, cf. Tables 3, 4, entries 7, 8). BIFOP-CN (**12**) affords similar results as BIFOP-N_3 (**11**, cf. Tables 3, 4, entries 5, 6). BIFOP-F (**9**) originates the stereochemical "F-switch" which is achieved for both substrates, yielding either (*R*,*E*)-dimethyl 2-(1,3-diphenylallyl)malonate (*R*)-**2** (92% with 66% ee, cf. Figure 1, Scheme 2, Table 3, entry 4) or (*S*)-dimethyl 2-(cyclohexenyl)malonate (*S*)-**4** (82% with 67 ee, cf. Figure 1, Scheme 3, Table 4, entry 4). NBO-analyzes reveals that the explanation of this "F-swtich" is a hyperconjugation effect (lp)Pd → σ*(P-O) or (lp)Pd → σ*(P-F) influenced by the high electronegativity of fluorine (Figure 8, Table 8). This gives rise to a switch in the transition structures of the favoured enantiomer by stabilizing hyperconjugation energy (e.g. less favoured **F**: TS-**2** ΔG_{rel} = 3.2 kcal/mol, to favoured **F**: TS-**1** ΔG_{rel} = 7.6 kcal/mol, Figure 8, Table 8; cf. experimental Scheme 2, Table 3, Scheme 3, Table 4). This "F-switch" demonstrates how electronegativity can be employed in ligand and catalyst design to control enantioselectivity in Pd-catalyzed allylic alkylations.

Computational section

All computations are performed with GAUSSIAN 16 Revision B.0118. Transition state structures are localized using the B3LYP functional[19] with the def2-SVP basis set[20]. Energies are refined using either the M06-2X functional[21] with the def2-TZVP basis set[20] or TPSS functional[22] with def2-TZVP basis set[20]. Grimme's dispersion (D3) with Becke-Johnson damping (BJ)23 is added. The ZPE scale factor is for B3LYP/def2-SVP 0.9912, M06-2X/def2-TZVP 0.9754 and TPSS/def2-TZVP 1.0020[24]. The computed pictures are generated with CYLview[25]. The NBO-analyzes are done with NBO6. All functions are implemented in the GAUSSIAN 16 program package.

Conflicts of interest

There are no conflicts to declare.

Acknowledgements

We are grateful to the Fonds der Chemischen Industrie (FCI) for financial support. We also want to thank the Deutsche Forschungsgesellschaft (DFG-GO-930-13) for funding as well as the BASF AG, Bayer AG, Evonic AG, Wacker AG, Raschig GmbH, Symrise GmbH, Solvay GmbH and the OMG group for generous support. We also thank the computing center of the University of Cologne (RRZK) for providing CPU time on the DFG-funded supercomputer CHEOPS, as well as for support. We want to thank *B.Sc.* Azar Jahanbakhsh for her extraordinary support in advanced ligand synthesis and crystallization, as well as *Dr.* Lars Packschies and *Dr.* Viktor Achter for the maintenance of the HPC systems. We like to thank *Dipl.-Ing.* Andreas Adler for HPLC and GC support and *Dr.* Matthäa Verena Holland-Cuntz for her exceeding support of the pioneer work of this paper.

References

1 (a) I. G. Rios, A. Rosas-Hernandez, E. Martin, Recent Advances in the Application of Chiral Phosphine Liganfs in Pd-Catalysed Asymmetric Allylic Alkylation. *Molecules* 2011, **16**, 970-1010; (b) Z. Lu, S. Ma, Metal-Catalyzed Enantioselective Allylation in Asymmetric Synthesis. *Angew. Chem. Int. Ed.* 2008, **47**, 258-297; (c) B. M. Trost, M. L. Crawley, Asymmetric Transition-Metal-Catalyzed Allylic Alkylations: Applications in Total Synthesis. *Chem. Rev.* 2003, **103**, 2921-2944.

2 (a) S. Kudis, G. Helmchen, Enantioselektive allylische Substitution an cyclischen Substraten unter Katalyse mit Palladiumkomplexen von P,N-Chelatliganden mit Cymantreneinheit. *Angew. Chem.* 1998, **110**, 3210-3212; Enantioselective Allylic Substitution of Cyclic Substrates by Catalysis with Palladium Complexes of P,N-Chelate Ligands with a Cymantrene Unit. *Angew. Chem. Int. Ed.* 1998, **37**, 3047-3050; (b) G. Helmchen, Enantioselective palladium-catalyzed allylic substitutions with asymmetric chiral ligands. *J. Organomet. Chem.* 1999, **576**, 203-214; (c) G. Helmchen, A. Pfaltz, Phosphinooxazolines – A New Class of Versatile, Modular P,N-Ligands for Asymmetric Catalysis. *Acc. Chem. Res.* 2000, **33**, 336-345; (d) M. Kollmar, B. Goldfuss, M. Reggelin, F. Rominger, G. Helmchen, (Phosphanyloxazoline)palladim Complexes, Part I: (η^3-1,3-Dialkylallyl)(phosphanyloxazoline)palladium Complexes: X-Ray Crystallographic Studies, NMR Investigations, and Quantum-Chemical Calculations. *Chem. Eur. J.* 2001, **7**, 4913-4927; (e) J. Vázquez, B. Goldfuss, G. Helmchen, Isomerism of (π-1,3-dimethylallyl)(phosphinooxazoline)Pd complexes: a comparison between experiment and theory. *J. Organomet. Chem.* 2002, **641**, 67-70; (f) M. Kollmar, H. Steinhagen, J. P. Janssen, B. Goldfuss, S. A. Malinovskaya, J. Vázquez, F. Rominger, G. Helmchen, (η^3-Phenylallyl)(phosphanyloxazoline)palladium Complexes:

X.Ray Crystallographic Studies, NMR Investigations, and Ab Initio/DFT Calculations. *Chem. Eur. J.* 2002, **8**, 3103-3114; (g) P. von Matt, A. Pfaltz, Chiral Phosphinoaryldihydrooxazoles as Ligands in Asymmetric Catalysis: Pd-Catalyzed Allylic Substitution. *Angew. Chem. Int. Ed.* 1993, **32**, 566-568; Chirale Phosphinoarylhydrooxazole als Liganden in der asymmetrischen Katalyse: Pd-katalysierte allylische Substitution. *Angew. Chem.* 1993, **105**, 614-615; (h) J. Sprinz, G. Helmchen, Phosphinoaryl- and phosphinoalkyloxazolines as new chiral ligands for enantioselective catalysis: Very high enantioselectivity in palladium catalyzed allylic substitutions. *Tetrahedron Lett.* 1993, **34**, 1769-1772; (i) J. G. Dawson, C. G. Frost, S. J. Coote, J. M. J. Williams, Asymmetric palladium catalysed allylic substitution using phosphorus containing oxazoline ligands. *Tetrahedron Lett.* 1993, **34**, 3149-3150; (j) J. M. J Williams, The Ups and Downs of Allylpalladium Complexes in Catalysis. *Synlett* 1996, 705-710.

3 B. Goldfuss, T. Löschmann, F. Rominger, Ligand Bite Governs Enantioselectivity: Electronic and Steric Control in Pd-Catalyzed Allylic Alkylations by Molecular Fenchyl Phosphinites (FENOPs). *Chem. Eur. J.* 2004, **10**, 5422-5427.

4 E. Brüllingen, J.-M. Neudörfl, B. Goldfuss, Enantioselective Cu-catalyzed 1,4-additions of organozinc and Grignard reagents to enones: exceptional performance of the hydrido-phosphite-ligand BIFOP-H. *New J. Chem.* 2019, **43**, 4787-4799.

5 (a) W. Neugebauer, A. J. Kos, P. V. R. Schleyer, Regioselektive dimetallierung von aromaten. Bequemer zugang zu 2,2'-disubstituierten biphenylderivaten. *J. Organomet. Chem.* 1982, **228**, 107-118; (b) B. Goldfuss, E. Eisenträger, Chiral ligand induced distortions: the origin of pyramidal three-coordinated lithium ions in the X-ray crystal structure of Lithium (1R,2R,4S)-exo-2-[o-(dimethylaminomethyl)phenyl]-1,3,3-trimethylbicyclo[2.2.1]heptan-endo-2-olate. *Aust. J. Chem.* 2000, **53**, 209-212; (c) B. Goldfuss, T. Löschmann, F. Rominger, Phosphinofenchol or Metastable Phosphorane? Phosphorus Derivatives of Fenchol. *Chem. Eur. J.* 2001, **7**, 2028-2033; (d) F. Soki, J.-M. Neudörfl, B. Goldfuss, Surprising fenchone induced cyclization: synthesis of the new chiral diol biphenyl-2,2'-sulfone-3,3'-bisfenchol (BISFOL). *Tetrahedron* 2005, **61**, 10449-10453; (e) D. Lange, J.-M. Neudörfl, B. Goldfuss, New chiral lithium aluminum hydrides based on biphenyl-2,2'-bisfenchol (BIFOL): structural analyses and enantioselective reductions of aryl ketones. *Tetrahedron* 2006, **62**, 3704-3709; (f) B. Goldfuss, S. I. Khan, K. N. Houk, Chiral Complexes with *n*-Butyllithium and Methylzinc: X-ray Crystal Structures of Lithium and Zinc (1R,2R,4S)-2-endo-Oxido-2-eco-(o-methoxyphenyl)-1,3,3-trimethylbicyclo[2.2.1]heptanes. *Organometallics* 1999, **18**, 2927-2929; (g) B. Goldfuss, M. Steigelmann, S. I. Khan, K. N. Houk, Rationalization of Enantioselectivities in Dialkylzinc Additions to Benzaldehyde Catalyzed by Fenchones Derivatives. *J. Org. Chem.* 2000, **65**, 77-82; (h) B. Goldfuss, M. Steigelmann, Structure and Reactivity of Chiral Fenchone Based Organozinc Catalysts. *J. Mol. Model.* 2000, **6**, 166-170; (i) B. Goldfuss, M. Steigelmann, F. Rominger, Increasing Enantioselectivities and Reactivities by Stereochemical Tuning: Fenchone-Based Catalysts in Dialkylzinc Additions to Benzaldehyde. *Eur. J. Org. Chem.* 2000, 1785-1792; (j) M. Steigelmann, Y. Nisar, F. Rominger, B. Goldfuss, Homo- and Heterochiral Alkylzinc Fencholates: Linear on Nonlinear Effects in Dialkylzinc Additions to Benzaldehyde. *Chem. Eur. J.* 2002, **8**, 5211-5218; (k) B. Goldfuss, M. Steigelmann, F. Rominger, Chirale Modifizierung von n-Butyllithium: Steuerung von Stöchiometrie, Struktur und Enantioselektivität durch modulare Fencholat-Einheiten. *Angew. Chem.* 2000, **112**, 4299-4302; Chirally Modified *n*-Butyllithium: Tuning the Composition, Structure, and Enantioselectivity with Modular Fencholates. *Angew. Chem. Int. Ed.* 2000, **39**, 4133-4136; (l) B. Goldfuss, M. Steigelmann, F. Rominger, H. Urtel, Chiral Modular *n*-Butyllithium Aggregates: *n*BuLi Complexes with Anisyl Fencholates. *Chem. Eur. J.* 2001, **7**, 4456-4464; (m) B. Goldfuss, Organolithiums in Enantioselective Additions to n* and σ* Carbon-Oxygen Electrophiles. *Synthesis* 2005, 2271-2280; (n) B. Goldfuss, M. Steigelmann, T. Löschmann, G. Schilling, F. Rominger, A Dispensable Methoxy Group? Phenyl Fencholate as a Chiral Modifier of *n*-Butyllithium. *Chem. Eur. J.* 2005, **11**, 4019-4023; (o) F. Soki, J.-M. Neudörfl, B. Goldfuss, Homo- vs. heterometallic organolithium fencholates: Structures and selectivities. *J. Organomet. Chem.* 2008, **693**, 2139-2146; (p) M. Leven, N. E. Schlörer, J.-M. Neudörfl, B. Goldfuss, Control of Enantioselectivity with Felxible Biaryl Axes: Terpene-Based Alkylzinc Catalysts in Enatioselective Dialkylzinc Additions. *Chem. Eur. J.* 2010, **16**, 13443-13449; (q) M. Leven, D. Müller, B. Goldfuss, Enantioselective Alkynylation of Aromatic Aldehydes: Pyridyl Phenylene Terpeneol Catalysts with Flexible Biaryl Axes. *Synlett* 2011, 2505-2508; (r) A. Gliga, H. Klare, M. Schumacher, F. Soki, J.-M. Neudörfl, B. Goldfuss, New Umpolung Catalysts: Reactivity and Selectivity of Terpenol-Based Lithium Phosphonates in Enantioselective Benzoin-Type Couplings. *Eur. J. Org. Chem.* 2011, 256-263; (s) V. Grote, J.-M. Neudörfl, B. Goldfuss, Enantiopure Methyl-Phenyllithium: Mixed (Carb-)Anionic Anisyl Fencholate-Aggregates. *Organomet.* 2019, **38**, 771-779; (t) F. Fox, J.-M. Neudörfl, B. Goldfuss, Silanediol versus chlorosilanol: hydrolyes and hydrogen-bonding catalyses with fenchole-based silanes. *Beilstein J. Org. Chem.* 2019, **15**, 167-186.

6 (a) B. Goldfuss, T. Kop-Weiershausen, J. Lex, J.-M. Neudörfl, An exceptional P-H phosphonite: Biphenyl- 2,2'-bisfenchylchlorophosphite and derived ligands (BIFOPs) in enatioselective copper- catalyzed 1,4-additions. *Beilstein J. Org. Chem.* 2005, **1**, 6-10; (b) B. Goldfuss, T. Löschmann, T. Kop-Weiershausen, J.-M. Neudörfl, F. Rominger, A superior P-H phosphonite: Asymmetric allylic substitutions with fenchol-based palladium catalysts. *Beilst. J. Org. Chem.* 2006, **2**, 7-11.

7 R. Blanco-Trillo, M. Leven, J.-M. Neudörfl, B. Goldfuss, Electronegativity Governs Enantioselectivity: Alkyl-Aryl Cross-Coupling with Fenchol-Based Palladium-Phosphorus Halide Catalysts. *Adv. Synth. Catal.* 2012, **354**, 1451-1465.

8 (a) M. Aufiero, R. Gilmour, Informing Molecular Design by Stereoelectronic Theory: The Fluorine *Gauche* Effect in Catalysis. *Acc. Chem. Res.* 2018, **51**, 1701-1710; (b) C. Thiehoff, Y. P. Rey, R. Gilmour, The Fluorine *Gauche* Effect: A Brief History. *Isr. J. Chem.* 2017, **57**, 92-100; (c) K. A. Lee, D. L. Silverio, S. Forker, D. W. Robbins, F. Haeffner, F. W. van der Mei, A. H. Hoveyda, Catalytic enantioselective addition of organoboron reagents to fluoroketones controlled by electrostatic interactions. *Nat. Chem.* 2016, **8**, 768-777; (d) C. Thiehoff, M. C. Holland, C. Daniliuc, K. N. Houk, R. Gilmour, Can acyclic conformational control be achieved *via* a sulfur-fluorine *gauche* effect? *Chem. Sci.* 2015, **6**, 3565-3571; (e) L. E. Zimmer, C. Sparr, R. Gilmour, Fluorine Conformational Effects in Organocatalysis: An Emerging Strategy for Molecular Design. *Angew. Chem. Int. Ed.* 2011, **50**, 11860-11871; (f) D. Cahard, V. Bizet, The influence of fluorine in asymmetric catalysis. *Chem. Soc. Rev.* 2014, **43**, 135-147; (g) V. Bizet, D. Cahard, Fluorine as a Control Element in Asymmetric Synthesis. *Chimia* 2014, **68**, 378-381.

9 J. C. R. Thacker, P. L. A. Popelier, Fluorine Gauche Effect Explained by Electrostatic Polarization Instead of Hyperconjugation: An Interacting Quantum Atoms (IQA) and Relative Energy Gradient (REG) Study. *J. Phys. Chem. A* 2018, **122**, 1439-1450.

10 (a) G. Poli, G. Giambastiani, A. Mordini, Palladium-Catalyzed Allylic Alkylations via Titanated Nucleophiles: A New Warly-Late Heterobimetallic System. *J. Org. Chem.* 1999, **64**, 2962-2965; (b) R. Šebesta, A. Škvorcová, Influence of structural changes in ferrocene phosphane aminophosphane ligands on their catalytic activity. *J. Organomet. Chem.* 2009, **694**, 1898-1902; (c) X. Cattoën, M. A. Pericàs, Synthesis of highly modular bis(oxazoline) ligands by Suzuki cross-coupling and evaluation as catalytic ligands. *Tetrahedron* 2009, **65**, 8199-8205.

11 Y. Sato, T. Yoshimo, M. Mori, N-Heterocyclic Carbenes as Ligands in Palladium-Catalyzed Tsuji-Trost Allylic Substitution. *J. Organomet. Chem.* 2005, **690**, 5753-5758.

12 (a) S. Anantharaj, U. Nithiyanantham, S. R. Ede, E. Ayyappan, S. Kundu, π-stacking intercalation and reductant assisted stabilization of osmium organosol for catalysis and SERS applications. *RSC Adv.* 2015, **5**, 11850-11860; (b) S. E. Wheeler, K. N. Houk, Substituent Effects in Cation/π Interactions and Electrostatic Potentials above the Centers of Substituted Benzenes Are Due Primarily to Through-Space Effects of the Substituents. *J. Am. Chem. Soc.* 2009, **131**, 3126-3127; (c) M. S. Marshall, R. P. Steele, K. S. Thanthiriwatte, C. D. Sherrill, Potential Energy Curves for Cation-π Interactions: Off-Axis Configurations Are Also Attractive. *J. Phys. Chem. A* 2009, **113**, 13628-13632; (d) J. C. Ma, D. A. Dougherty, The Cation-π Interaction. *Chem Rev.* 1997, **97**, 1303-1324.

13 R. Blanco-Trillo, J.-M. Neudörfl, B. Goldfuss, An unusually stable chlorophosphite: What makes BIFOP-Cl so robust against hydrolysis? *Beilstein J. Org. Chem.* 2016, **11**, 313-322.

14 M. Coll, O. Pàmies, M. Diéguez, Highly Versatile Pd-Thioether-Phosphite Catalytic Systems for Asymmetric Allylic Alkylation, Amination, and Etherification Reactions. *Org. Lett.* 2014, **16**, 1892-1895.

15 L. P. Wolters, F. M. Bickelhaupt, Nonlinear d^{10}-ML_2 Transition Metal Complexes. *ChemistryOpen* 2013, **2**, 106-114.

16 F. Weinhold, C. R. Landis, Discovering Chemistry With Natural Bond Orbitals. 2012, John Wiley & Sons, Inc. Hoboken, New Jersey.

17 (a) I. V. Alabugin, S. Bresch, G. dos Passos Gomes, Orbital hybridization: a key electronic factor in control of structure and reactivity. *J. Phys. Org. Chem.* 2015, **28**, 147-162; (b) H. A. Bent, An Appraisal of Valence-bond Structures and Hybridization in Compounds of the First-row elements. *Chem. Rev.* 1961, **61**, 275-311.

18 Gaussian 16, Revision B.01, M. J. Frisch, G. W. Trucks, H. B. Schlegel, G. E. Scuseria, M. A. Robb, J. R. Cheeseman, G. Scalmani, V. Barone, G. A. Petersson, H. Nakatsuji, X. Li, M. Caricato, A. V. Marenich, J. Bloino, B. G. Janesko, R. Gomperts, B. Mennucci, H. P. Hratchian, J. V. Ortiz, A. F. Izmaylov, J. L. Sonnenberg, D. Williams-Young, F. Ding, F. Lipparini, F. Egidi, J. Goings, B. Peng, A. Petrone, T. Henderson, D. Ranasinghe, V. G. Zakrzewski, J. Gao, N. Rega, G. Zheng, W. Liang, M. Hada, M. Ehara, K. Toyota, R. Fukuda, J. Hasegawa, M. Ishida, T. Nakajima, Y. Honda, O. Kitao, H. Nakai, T. Vreven, K. Throssell, J. A. Montgomery, Jr., J. E. Peralta, F. Ogliaro, M. J. Bearpark, J. J. Heyd, E. N. Brothers, K. N. Kudin, V. N. Staroverov, T. A. Keith, R. Kobayashi, J. Normand, K. Raghavachari, A. P. Rendell, J. C. Burant, S. S. Iyengar, J. Tomasi, M. Cossi, J. M. Millam, M. Klene, C. Adamo, R. Cammi, J. W. Ochterski, R. L. Martin, K. Morokuma, O. Farkas, J. B. Foresman, and D. J. Fox, Gaussian, Inc., Wallingford CT, 2016; GaussView, Version 6, R. Dennington, T. A. Keith, J. M. Millam, Semichem Inc., Shawnee Mission, KS, 2016.

19 For B3 see: (a) A. D. Becke, Density-functional thermochemistry. III. The role of exact exchange. *J. Chem. Phys.* 1993, **98**, 5648-5652; for LYP see: (b) C. Lee, W. Yang, R. G. Parr, Development of the Colle-Salvetti correlation-energy formula into a functional of the electron density. *Phys. Rev. B* 1988, **37**, 785-789; for VWN see: (c) S. H. Vosko, L. Wilk, M. Nusair, Accurate spin-dependent electron liquid correlation energies for local spin density calculations: a critical analysis. *Can. J. Phys.* 1980, **58**, 1200-1211; for an assembly see: (d) P. J. Stephens, F. J. Devlin, C. F. Chabalowski, M. J. Frisch, Ab Initio Calculation of Vibrational Absorption and Circular Dichroism Spectra Using Density Functional Force Fields. *J. Phys. Chem.* 1994, **98**, 11623-11627.

20 F. Weigend, R. Ahlrichs, Balanced basis sets of split valence, triple zeta valence and quadruple zeta quality for H to Rn: Design and assessment of accuracy. *Phys. Chem. Chem. Phys.* 2005, **7**, 3297-3305.

21 Y. Zhao, D. G. Truhlar, The M06 suite of density functional for main group thermochemistry, thermochemical kintetics, noncovalent interactions, excited states, and transition elements: two new functional and systematic testing of four M06-class functional and 12 other functional. *Theor. Chem. Acc.* 2008, **120,** 215-241.

22 J. Tao, J. P. Perdew, V. N. Staroverov, G. E. Scuseria, Climbing the Density Functional Ladder: Nonempirical Meta-Generalized Gradient Approximation Designed for Molecules ans Solids. *Phys. Rev. Lett.* 2003, **91**, 146401-1-146401-4.

23 S. Grimme, S. Ehrlich, L. Goerigk, Effect of the damping function in dispersion corrected density functional theory. *J. Comp. Chem.* 2011, **32**, 1456-1465.

24 M. K. Kesharwani, B. Brauer, J. M. L. Martin, Frequency and Zero-Point Vibrational Energy Scale Factors for Double-Hybrid Density Functionals (and Other Selected Methods): Can Anharmonic Force Fields Be Avoided?. *J. Phys. Chem. A* 2015, **119**, 1701-1714.

25 C. Y. Legault, CYLview, 1.0b; Université de Sherbrooke 2009 (http://www.cylview.org).

Manuscript ID NJ-ART-05-2019-002798

View Article Online
DOI: 10.1039/C9NJ02798J

Entry for the Table of Contents

Ligand's Electronegativity Controls Sense of Enantioselectivity in BIFOP-X Palladium-Catalyzed Allylic Alkylations